We are IntechOpen,
the world's leading publisher of
Open Access books
Built by scientists, for scientists

6,900
Open access books available

186,000
International authors and editors

200M
Downloads

Our authors are among the

154
Countries delivered to

TOP 1%
most cited scientists

12.2%
Contributors from top 500 universities

CLARIVATE ANALYTICS
BOOK CITATION INDEX
INDEXED

WEB OF SCIENCE™

Selection of our books indexed in the Book Citation Index
in Web of Science™ Core Collection (BKCI)

Interested in publishing with us?
Contact book.department@intechopen.com

Numbers displayed above are based on latest data collected.
For more information visit www.intechopen.com

The Role of the Purkinje System in Defibrillation

Edward J Vigmond[1], Patrick M. Boyle[1] and Makarand Deo[2]
[1]University of Calgary
[2]University of Michigan
[1]Canada
[2]U.S.A.

1. Introduction

Only relatively recently have we begun to understand how defibrillation shocks work on the mechanistic level (Cheng et al., 1999; Trayanova & Skouibine, 1998). Virtual electrode polarization has offered a plausible mechanism for explaining far field effects of defibrillation shocks. However, this body of work has not considered the role of the specialized cardiac conduction system, the Purkinje System (PS), in the defibrillation process.

Despite its crucial role in activation, relatively little is known about the role of the PS in defibrillation. This is due to several factors which make recording from it challenging: The PS is a fine structure lying on the endocardium which makes it difficult to see and impale with microelectrodes. While Langendorf preparations allow easy access to the epicardium for optical recordings, the PS lies on the endocardium and is, therefore, much harder to access while maintaining the integrity of the ventricles. Depending on species, the PS penetrates various depths into the myocardium, masking midmyocardial activation. Plunge electrodes are one option for recording from the midmyocardium, but amplifier saturation immediately following large shocks would lose important information. Since the PS fibres are fine, the signals produced by them are very small and get easily swamped by signals from the myocardium. This is true for both electrical and optical recordings. Computer modelling, therefore, offers an attractive platform for studying the role of the PS in defibrillation, since the electrical activity everywhere in the system is known and can be visualized.

2. Description of the Purkinje System

The specialized conduction system begins at the atrioventricular node with the bundle of His. The His bundle runs through the ventricular septum, and bifurcates into the left and right Tawara branches, which further subdivide into major fascicles and later form a network on the endocardial surface. There are three major fascicles in the left ventricle, and two in the right.

A large portion of the conduction system is located within the ventricular cavities and is termed free running. Fibres that run within the ventricular walls are very difficult to visualize, requiring histological examination. Referring to the PS network as a tree is incorrect since, unlike true tree structures, fibres follow paths which join back together and at the final level,

forming more of a mesh-like topology. This may give redundancy to the network so that a part of the PS may fail without comprising sinus activation.

Segments of the PS run as bundles wrapped in collagen sheaths. This is easily seen in the bundle of His, which is a large trunk of many fibres. At branch points of thicker fibre bundles, individual fibres do not bifurcate. However, in the distal PS, where a network segment may be formed from a few fibres, individual fibres may branch. Longitudinal coupling is very strong, while lateral connections are sparser.

The PS is electrically isolated from the myocardium except for the termini of the network, where Purkinje-Myocyte Junctions (PMJs) are formed. While the PS can be selectively stained and visualized on the endocardium, determining PMJ locations is difficult. PMJs may be located well within the ventricular wall, which means that histological examination is necessary. Currently, the number of functional PMJs is not well characterized. Although the density of the PS on the endocardium appears high, the number of penetrating segments is unknown, as is the number of PMJs that successfully transmit pulses (Morley et al., 2005).

There are significant species differences in the degree of transmural penetration of terminal PS fibres. Species can roughly be grouped into three categories (Canale et al., 1986): Group 1 comprises the ungulates which have deeply penetrating fibres, reaching almost to the epicardium. Group 2 includes primates and carnivores which have PS termini that penetrate about 1/3 of the way through the wall. Group 3 contains rodents with very little penetration of the PS into the myocardial wall. This factor may be especially important for interpreting experimental results between species.

3. Modeling methods

Modelling the reaction of the of the ventricles and PS to defibrillation shocks is a computationally demanding task since the timestep during the defibrillation pulse must be very small. This is because high field strengths induce rapid changes in model parameters, and numerical instabilities may develop Vigmond et al. (2008). Lastly, ionic models are developed under normal physiological conditions. Defibrillation shocks are outside the bounds of the models developed so additional measures need be taken such as adding an ionic current to properly account for high voltage responses Ashihara & Trayanova (2004).

The bidomain equations are the most complete macroscopic description of cardiac tissue, even being predictive of polarization patterns(Sepulveda et al., 1989) induced by extracellular stimulation. They can be cast into a elliptical and parabolic equation:

$$\nabla \cdot (\overline{\sigma}_i + \overline{\sigma}_e)\nabla\phi_e = -\nabla \cdot \overline{\sigma}_i\nabla V_m - I_e \qquad (1)$$

$$\nabla \cdot \overline{\sigma}_i\nabla V_m = -\nabla \cdot \overline{\sigma}_i\nabla\phi_e + \beta I_m \qquad (2)$$

where subscripts i and e denote intra- or extracellular quantities respectively, ϕ is potential, $\bar{\sigma}$ is the conductivity tensor, I_e is an applied extracellular stimulus current, β is the surface to volume ratio, and I_m is the transmembrane current. Another set of ordinary differential equations is required to model the flow of the ions across the cell membrane and is embedded in I_m. These equations can be solved using an operator splitting method where extracellular potential (Eqn. 1), ionic currents, and the transmembrane voltage (Eq. 2 are solved sequentially (Vigmond et al., 2008).

The system is solved by using the finite element method. In our simulations, rabbit ventricular geometry (Vetter & McCulloch, 1998) was discretized at approximately 350 μm resolution resulting in about 550,000 nodes comprising the myocardium and another 300,000 nodes comprising the cavities and a surrounding bath. The PS was modelled as a network of one dimensional cubic Hermite finite elements added within the myocardial mesh (Vigmond & Clements, 2007). Two methods have been used to generate PSs for computer modelling studies: One approach is more generic and does not rely on mapping a particular PS. The endocardia of the two ventricles are unrolled and the PS drawn on according to basic physiological principles outlined in the preceding section (Vigmond & Clements, 2007). A fractal method could be used to further increase the endocardial mesh density (Ijiri et al., 2008). The second approach uses high resolution imaging to reconstruct the free running PS (see Fig. 1). This may further be augmented by staining the PS to reveal the endocardial mesh. With either method, the insertion of the PS into the myocardium must follow a rule-based method since the PS cannot be imaged within the myocardium, but requires careful histological examination, electron microscopy or genetic tagging (Miquerol et al., 2004). to reveal its transmural course (Ono et al., 2009). Furthermore, while the endocardial network appears dense, the number of functional PMJs is far less (Morley et al., 2005). The one-dimensional cubic Hermite finite elements are only electrically connected to the myocardium at end points through gap junctions. Due to their higher polynomial order, cubic Hermite elements possess the property that they can enforce current continuity at junctions, as well as at PMJs. Discretization of the PS was at the cellular length level with discrete gap junctions.

Since the discretization of the finite element model is much coarser than the actual physical PMJ structure, a phenomenological approach is followed whereby a single PS terminus stimulates a volume of myocardium. The current flowing from the PS into a myocardial node is given by

$$i_{PMJ} = \frac{1}{R_{PMJ}} (V_m^{PS} - V_m^{myo}) \tag{3}$$

and i_{PMJ} is treated as an intracellular stimulus by the myocardium.

From the PS perspective, the currents are handled as explicit boundary conditions:

$$i_L = \frac{1}{K R_{PMJ}} \sum_j (V_m^{PS} - V_{m,j}^{myo}) i_L = \tag{4}$$

where j is the set of myocardial nodes coupled to a PS terminus, and K is a scaling factor which accounts for the current amplification by transitional cells which occurs at scales finer than that discretized. By setting R_{PMJ} and K, it is possible to recreate asymmetric propagation across the PMJ with an anterograde transmission delay on the order of 5 ms and retrograde transmission delay on the order of 1 ms as observed experimentally Huelsing et al. (1998); Wiedmann et al. (1996).

4. Role in fibrillation

It is important to first understand the role of the PS in fibrillation. It has been implicated as a major player in the initiation and maintenance of fibrillation. First, the PS can be a

source of focal firing. Chemical ablation of the PS by Lugol's solution, to selectively remove the endocardial layer and the PS embedded within it, has been shown to greatly diminish repetitive endocardial focal discharges and eliminate sustained VF (Wu et al., 2009). Part of this comes from the intrinsic nature of the Purkinje cells, which are resistant to ischemia because of large glycogen stores (Streit, 1987). This is especially important in long duration VF, at which point much of the myocardium has been compromised.

Second, the PS can provide alternative pathways for reentrant pathways. This is supported by experiments wherein chemical ablation of the PS has also been shown to reduce the inducibility of ventricles to VF(Armiger & Knell, 1988; Dosdall et al., 2008) In agreement, computer simulations have also shown an increase in VF vulnerability to large shocks when a PS is present (Deo et al., 2009). Several factors were identified which were responsible for the arrhythmogenic influence of the PS: 1) The presence of a PS produces more activations, which directly lead to reentrant activity. 2) The frequency of scroll waves is increased since the PS accelerates conduction. This acceleration may be visible as a breakthrough occurring ahead of the wavefront, or it may not be visible since the breakthroughs become coincident with the wavefront. This latter synchronization of activity starts to occur after several cycles. 3) Refractory tissue forms small islands around the PMJs, which induce more wavebreaks when a wavefront tries to propagate through the region. Finally, 4) the PS can provide escape pathways for wavefronts which would otherwise die by running into refractory tissue.

The PS affects fibrillation in many ways. Exposure to a large shock may disrupt pathways through the PS to terminate reentry, or ectopically firing PS cells may be reset. Disruption by an external shock may, therefore, influence reentrant activity but exactly how these factors relate remains to be elucidated.

5. Response to electric fields

The response of myocardial tissue to a strong electric shock depends on the orientation of the cells with respect to the electric field and how conductivity changes with respect to the direction of the electric field. This is seen in the expression for the generalized activating function, S (Sobie et al., 1997):

$$S = \mathbf{G_i} : \nabla(\nabla\phi_e) + (\nabla \cdot \mathbf{G_i}) \cdot \nabla\phi \tag{5}$$

where the colon signifies the matrix inner product. Looking at the two terms, activation can result from a gradient in the electric field, or from the irrotational portion of the conductivity field. Conductivity must be defined as a spatially-dependent tensor since its directional properties are determined by cellular orientation, which varies throughout the heart. This directional dependence arises from gap junction connectivity, which allows current to most easily flow longitudinally and experiences the highest resistance flowing across laminar sheets (Legrice et al., 1997).

The PS is essentially a network of one dimensional cables which repeatedly bifurcate and unify. In addition to the complex topology, the PS fibres undergo sudden changes in direction, as well as have termini which abruptly end. These properties all get reflected in the conductivity tensor. The complicated path of the fibres ensures that at least part of the PS is aligned in such a way as to be excited by the applied electric field. The end of the fibre is an abrupt discontinuity to zero conductivity outside of the fibre. Terminal

fibre segments which are aligned with the electric field will, therefore, have transmembrane potentials induced. Ends which face the cathode will be depolarized while ends facing the anode will be hyperpolarized.

The effect of field stimulation is shown in Fig. 1, where an MRI-derived isolated rabbit PS is exposed to shocks. The normal activation pattern is shown for reference, where it can be seen that it takes more than 30 ms for the entire network to be excited. When a shock is applied, many regions are excited simultaneously, not just one. This greatly abbreviates the excitation time of the tree and consequently, will result in near synchronous activation of the myocardium.
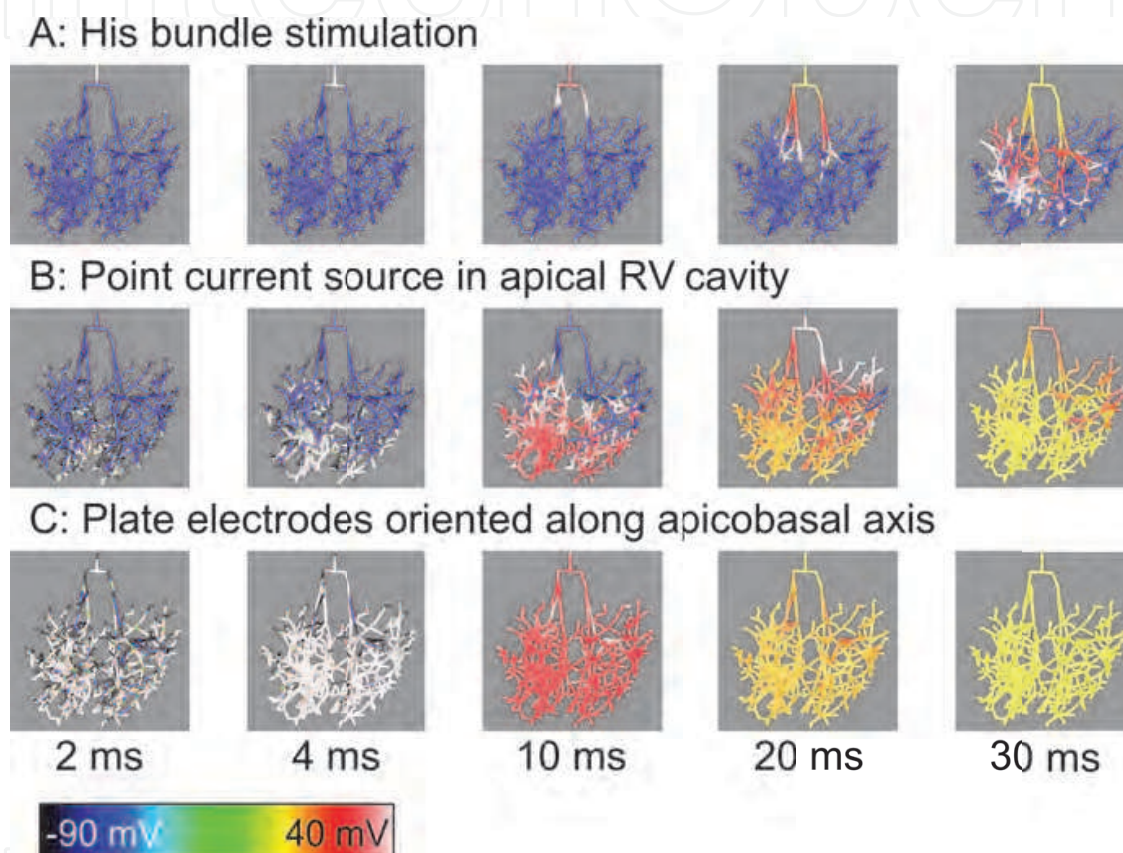
Fig. 1. Response of MRI-derived rabbit Purkinje System to electric fields. **A**: Normal activation starting at the proximal His bundle. **B**: 2.5 ms 125 mA point current source in the right ventricle **C**: 3 ms uniform 5 V/cm field oriented along the major axis of the heart. Color indicates transmembrane voltage. Times are given relative to stimulus onset.

Even on the cellular level, the PS reacts differently to high voltage shocks compared to ventricular myocytes. Using a papillary muscle preparation, Li et al. (1993) found that above a field strength of 20 V/cm, shocks induced a baseline shift and high frequency bursting in PS cells. In contrast, the ventricular myocytes entered a refractory state immediately after large shocks.

Thus, the PS is easily excited by electric field. Due to its one-dimensional nature and complex fibre trajectories, some part of it is always in a position to be excited by the field. This leads to rapid activation of the PS and, hence, of the myocardium connected through the PMJs. This
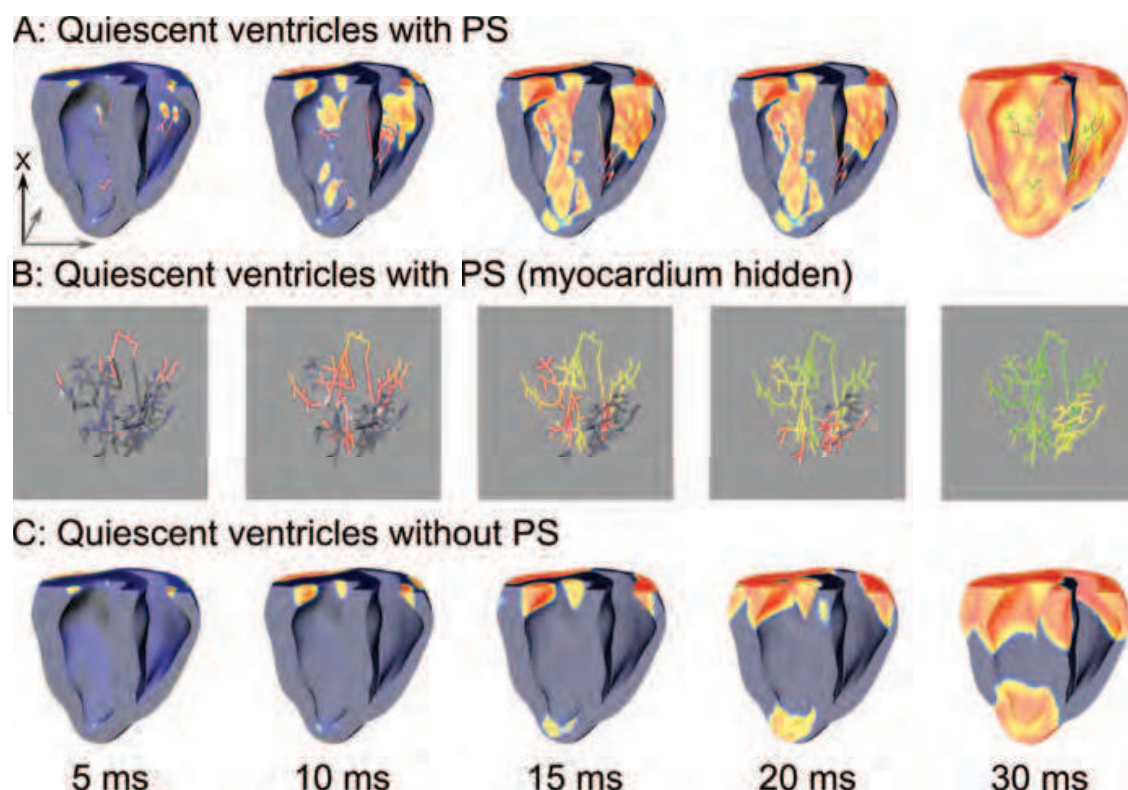
Fig. 2. **Response of the quiescent ventricles and PS to a** $2.5\,V/cm$ **shock.** Field orientation is along the long axis, as shown in A. When the PS is present, additional far-field activations can be seen on the endocardial surface.

will tend to be antiarrhythmic since the excitable gaps, which allow activity to keep exciting recovered tissue, will be more quickly consumed.

6. Quiescent ventricle studies

Simulations of the application of defibrillation-strength shocks to the quiescent ventricles with and without PS allow for the contribution of the PS to be identified. When stimulation is applied, large polarization gradients form in segments of the PS that are parallel to the electric field. The myocardium is also subject to excitation by direct and virtual electrode stimuli, but activation patterns in the two tissues do not necessarily coincide since PS fibres do not always run in the same direction as underlying ventricles cells. Furthermore, current flow in PS fibres is physically constrained and excitation spreads rapidly through the network, so even very weak shocks produce rapid excitation of the entire network. Thus, under the right circumstances, the contribution of the PS to the response of the quiescent ventricles can be remarkable.

Consider Fig. 2, where a $2.5\,V/cm$ field is applied along the long axis of the heart (from apex to base). Far-field excitations on the endocardial surface due to anterograde transmission of shock-induced activity in the PS is clearly visible (A); the presence of these effects is due to rapid propagation in the PS (B) and the relative lack of myocardial excitation from the field, which can be seen explicitly in the ventricles-only response (C). Consequently, the total ventricular activation time (t_{act}) is dramatically abbreviated.

	X			Y			Z		
	PS^+	PS^-	% ↓	PS^+	PS^-	% ↓	PS^+	PS^-	% ↓
−2.5 V/cm	55.7	100.1	44.3	29.3	29.8	1.6	28.4	29.1	2.2
+2.5 V/cm	41.1	63.1	34.8	26.1	26.9	3.2	28.2	29.4	4.1
−5 V/cm	43.1	67.0	35.6	28.3	28.4	0.1	28.2	28.3	0.3
+5 V/cm	33.6	57.3	41.4	24.6	24.8	1.0	27.5	27.7	0.7
−7.5 V/cm	37.3	42.4	12.1	28.2	28.2	0.2	28.5	28.3	0.5
+7.5 V/cm	30.7	38.3	19.9	22.6	23.2	2.2	27.6	27.7	0.3
−10 V/cm	30.0	36.1	17.0	28.4	28.3	0.3	28.1	28.0	0.5
+10 V/cm	30.1	34.5	12.6	22.4	22.4	0.0	27.8	27.9	0.2

Table 1. **Total activation time (t_{act}) with and without PS.** t_{act} was measured between the beginning of the shock and complete ventricular activation for four shock strengths in six directions, as described in the text.

In terms of t_{act}, the contribution of the PS to the response of the quiescent ventricles is only significant in cases where myocardial tissue in the vicinity of Purkinje-myocardial junctions (PMJs) is not excited by the shock. For the simulations discussed here, three orthogonal orientations were tested–along the long axis (X), across the septum (Y), and along the septum. As shown in the tabulated results for all simulations (Tab. 1), significant t_{act} abbreviation was only observed for shocks in the X direction.
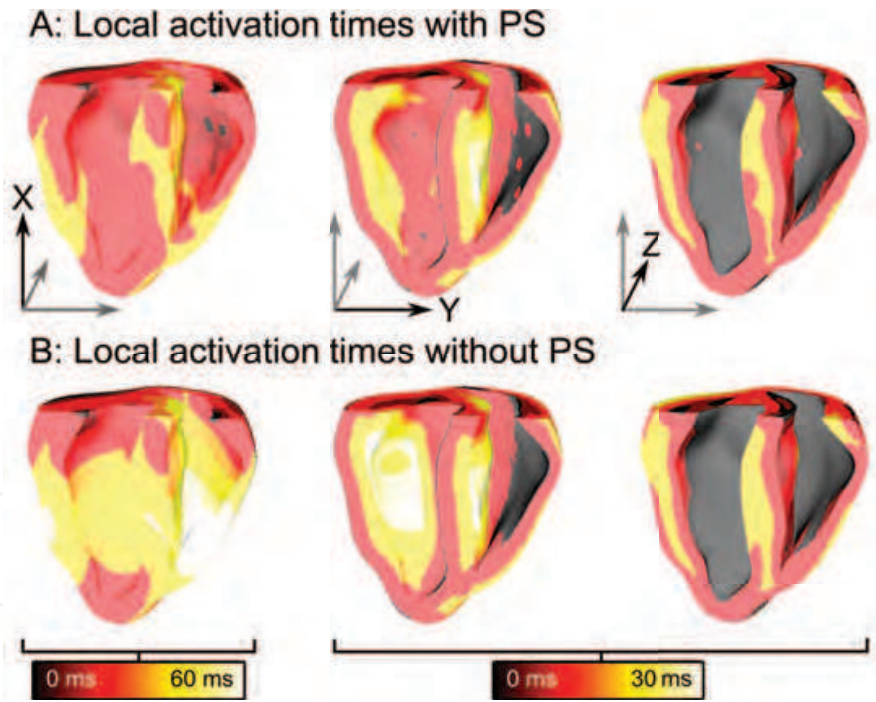

Fig. 3. **Local activation times for different field orientations,** $2.5 V/cm$ **shock.** Early activations due to PS activation make the biggest difference for shocks in the X direction, where myocardium near the PS is not significantly activated by the field. For shocks in the Y and Z differences, the PS causes some regions to activate much earlier (i.e. LV endocardial free-wall for Y), but overall activation time is not significantly abbreviated.

Interestingly, while the PS did not have a significant effect on t_{act} for shocks in the Y and Z directions, it did sometimes alter the pattern of local activation. For example, as shown in

Fig. 3, a weak shock in the Y direction resulted in much earlier activation of the LV endocardial free-wall due to PS excitations. Although t_{act} did not differ between simulations with and without the PS in this case, the modified order of activation could have consequences on subsequent beats due to gradients in refractoriness that might arise from local heterogeneity.
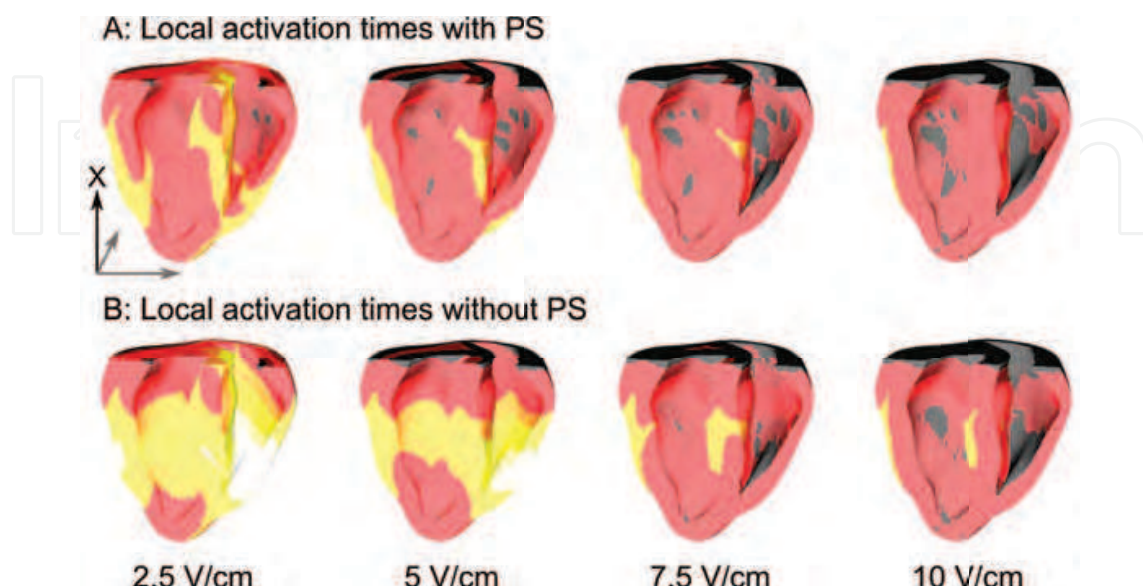

Fig. 4. **Local activation times for different field strengths along the long axis.** As shock strength increases, the role of the PS in the response of the quiescent ventricles is diminished, since the field causes excitation in a larger amount of myocardium. For the strongest shock (10 V/cm) only a few regions near PMJs, particularly in the septal region, contribute to t_{act} abbreviation. Stronger shocks abbreviate the activation delay between coupled PS and ventricular cells.

Increasing shock strength resulted in larger regions of myocardial polarization from the field, which effectively reduced the importance of the PS contribution in the response; this accounts for the diminishing returns in t_{act} abbreviation for shocks in the X direction, which is obvious in Tab. 1. As shown in Fig. 4, for the strongest shocks along the long axis simulated in this study, the primary source of t_{act} abbreviation was early activation of the septum, which is not easily excited by such shocks.

Interestingly, increased shock strength seemed to hasten the local effects of PS on endocardium. For example, in Fig. 4A, consider the dark regions on the endocardial surfaces, which are associated with early activation due to PS excitation. As the strength of stimulation increases (left to right), these regions become darker and larger, suggesting an abbreviation of anterograde transmission delay, perhaps due to the larger gradients in polarization. These observations were confirmed by inspecting voltages at the junctional voltage level (not shown), where the delay between coupled PS and ventricular cell upstroke was found to be almost uniformly shorter for larger shocks.

7. Isoelectric window

In general, shocks above a certain minimal strength result in sustained reentry; however, there is also a threshold for a maximum strength above which reentry is not induced. This Upper Limit of Vulnerability (ULV) is an important measure since it tends to correspond to

the Defibrillation Threshold (DFT)–the minimum shock strength necessary to halt ventricular fibrillation(Chen, Shibata, Dixon, Martin & Ideker, 1986). The ULV is particularly valuable as an easier to find surrogate measurement for DFT. Thus, insights on the ULV will provide insight on the DFT, which is of direct clinical importance.

Following failed defibrillation shocks near the ULV, there is a period of time during which new activity is not seen on the epicardium.(Chen, Shibata, Dixon, Wolf, Danieley, Sweeney, Smith & Ideker, 1986) This Isoelectric Window (IW) can be considerable, on the order of tens of milliseconds. It ends when activations break through on the epicardium and reentry resumes. Many long-standing questions surround this phenomenon: What is the nature of concealed activity during the IW? What is the mechanism that allows it to remain hidden for such a long time? Some researchers have argued that the PS plays an important role;(Dosdall et al., 2010) others have proposed the tunnel propagation theory, which suggests that cardiac surfaces are driven into refractory states and post-shock activity is confined to a thin transmural space with no excitable path to the epicardium.(Ashihara et al., 2008; Constantino et al., 2010) Some time later, the surface tissue recovers from refractoriness and activations break through. While the computer simulations carried out to construct this hypothesis were carefully constructed, it must be noted that they did not include a model of the PS.

For the purpose of comparison, we performed a set of simulations with the PS. A cross-shock protocol was applied with the second shock near the ULV to identify possible contributions of the PS during the IW. First, the ventricles were excited, either by transmembrane stimulation at the apex or by His bundle current injection. The former emulates experimental preparations while the latter results in a more physiological excitation pattern. During ventricular repolarization, a shock with appropriate strength and timing to induce arrhythmia was delivered by parallel plates, with the extracellular electric field oriented along the short axis of the heart.

7.1 Effects of varying coupling intervals and shock strengths on IW

Fig. 5 shows IW duration within the window of vulnerability for various combinations of shock timing–i.e. the coupling interval (CI)–and strength. For the AP+PS pre-shock configuration (A), the average IW decreased from 36 to 21 ms as CI increased from 145 to 155 ms. Similar IW gradients were seen for decreasing CI within the AP-PS (B) and His (C) configurations, from 49 to 34 ms and from 37 to 19 ms, respectively.

A similar trend was observed for increasing shock strength. In the AP+PS and His cases, where IW duration was determined by the time between the shock and the first PS-to-myocardial activation, the average IW decreased with increasing shock strength. For AP+PS, shocks ranging from 3.3 to 9 V/cm produced average IWs between 33 and 23 ms; for increasing shock strengths within the His configuration, IWs decreased from 31 to 20 ms. In the AP-PS configuration, where IW duration was determined by the spread of shock-induced activations in the apical region, average IW was reduced from 47 to 34 ms as shock strength increased from weakest to strongest. In the AP+PS and His cases, the PS was actively involved in the generation of first post-shock activity, so it was unsurprising that the IW was shorter than in AP-PS, where the PS was absent. This observation supports the hypothesis that the PS plays an important role in the immediate response to defibrillation shocks.
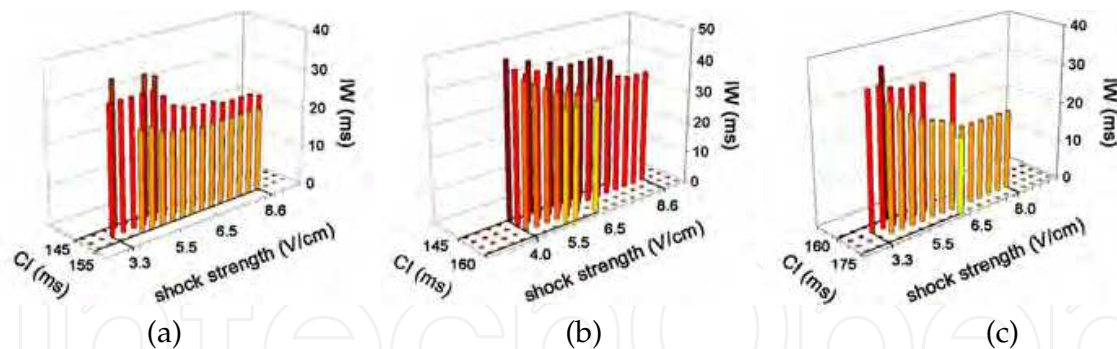
Fig. 5. IW duration for various combinations of shock strength and timing for three reentry induction protocols: (A) apical pacing with the PS (AP+PS), (B) apical pacing without the PS (AP-PS), and (C) His pacing. In general, longer CIs lead to shorter IWs.

7.2 First post-shock activation and the IW period

Activations were always observed in the PS immediately following the shock. During AP+PS runs, the first post-shock myocardial activation emanated from the PS 11 ms after the shock. After 15 ms, significant endocardial activation had occurred, as shown in Fig. 6(a). This is shorter than clinically-observed IWs due to the significant delay during which excitation propagates from the site of transmission to the epicardium. Fig. 6(b) shows the appearance of PS activations on the epicardium 23 ms after the shock; in most shocks applied to models with the PS during the vulnerable period, this pattern of excitation led to the first epicardial breakthrough. Note that the epicardial activation site is immediately opposite the endocardial PS insertion point. Mechanistically, the first PS activation initiated an endocardial rotor, which led to an epicardial activation (black arrow in Fig. 6); the underlying pattern of transmural activation is clearly shown.

As discussed earlier in this chapter, the distinct physiology and geometry of the PS lead to different polarization patterns than in the myocardium; in these simulations, the earliest post-shock activation was always observed within the PS. Excitation spread rapidly through the network and coupled myocardial tissue was activated by anterograde transmission. Thus, the first post-shock ventricular activation always emanated from the PS. In simulations without the PS, large gradients were induced near the apical region, leading to post-shock wavefronts.

Most experimental studies that reported an IW after defibrillation-level shocks mapped only epicardial or endocardial surfaces. Recently, Dosdall et al. (Dosdall et al., 2007) observed epicardial and subepicardial activations in pigs soon after shocks. Since the PS in pigs exhibits full transmural insertion (Chattipakorn et al., 2003), it is plausible that these mapped activations were first post-shock excitations provided by the PS. Furthermore, the earliest myocardial activations recorded were preceded by Purkinje potentials, which is in agreement with our findings. To the best of our knowledge, this is the first attempt to map PS activations following defibrillation. While limited spatial resolution prevented the authors from stating a clear conclusion, the results suggest that our simulation results are a step in the right direction. Other studies have observed endocardial or intramural activations that broke through to the epicardium 42 ms post-shock in sheep hearts (Evans & Gray, 2004). Given the fact that the PS terminates in the subendocardium in sheep,(Ansari et al., 1999) these observations are also
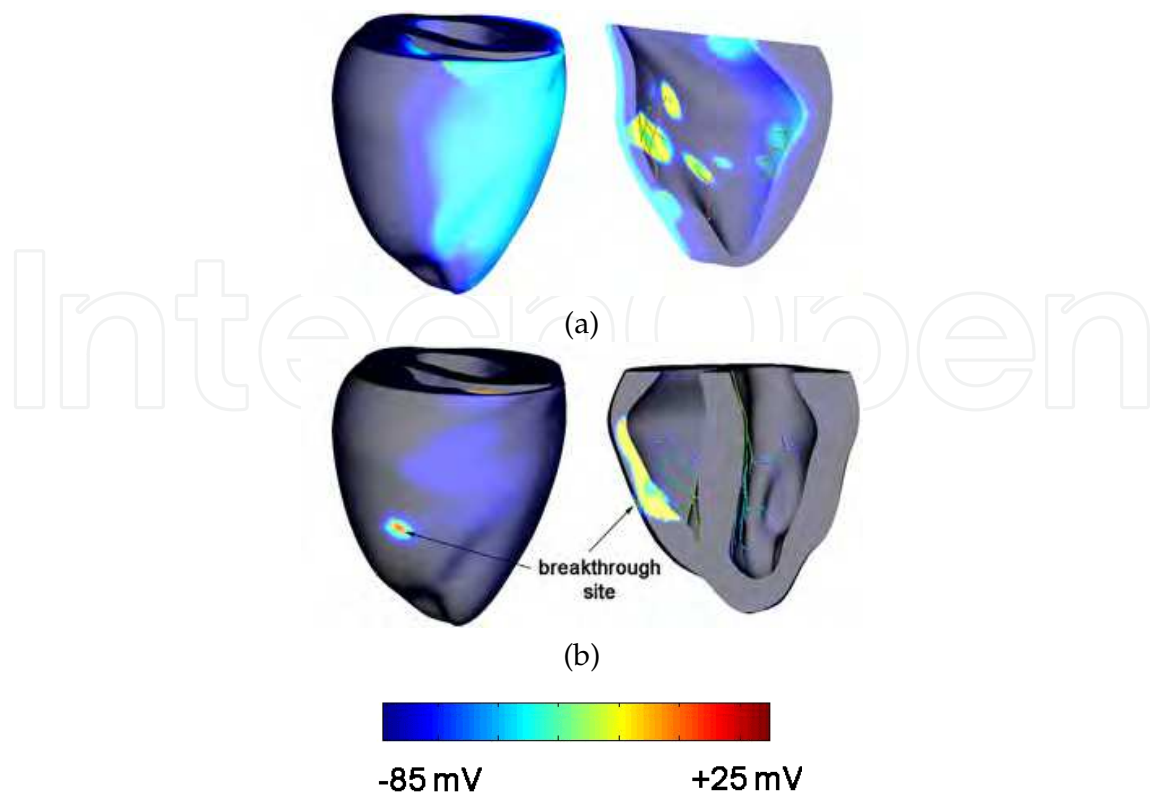
Fig. 6. Earliest postshock activation. (a) The first activation emanating from the PS 15 ms after the shock is clearly seen in the endocardial cross-section. (b) After 23 ms, the PS activation provides a focal breakthrough on the epicardium. Note the breakthrough site (arrow) is situated opposite the PS insertion point. Transmural depolarization due to the earliest postshock activation is evident. The right panel of (a) shows the LV endocardial free wall while the right panel of (b) shows a cross-section perpendicular to the septum with the posterior surface hidden.

consistent with our findings. Our study involves a smaller heart size, which explains the reduced IW durations compared to experimental values discussed here.

In our simulations, the PS was always strongly excited by the shock. In some cases, we observed midwall excitations similar to those observed in tunnel propagation studies.(Ashihara et al., 2008; Constantino et al., 2010) These were isolated by surface refractoriness, with excitable tissue confined to intramural paths. However, activations that originated in the PS broke through more quickly than purely myocardial midwall excitations, as shown in Fig. 7. Rapid conduction in the PS ensured that this happened consistently.

To further test our hypothesis that the PS was the source of epicardial breakthroughs following the IW, we changed the transmural insertion depth of PS endpoints. Figure 8 shows that the IW duration is dramatically reduced when the PS penetrates to the subepicardial layer. This is consistent with the PS being the primary source of post-shock epicardial activations due to rapid field-induced activations: deeper penetration brings PS fibres closer to the epicardium, so it makes sense that the IW is shorter. We observed that IW duration varied from 12 ms (full insertion) to 30 ms (no insertion). Epicardial breakthrough sites remained the same in all simulations for a given insertion depth; these sites were consistently situated opposite PS
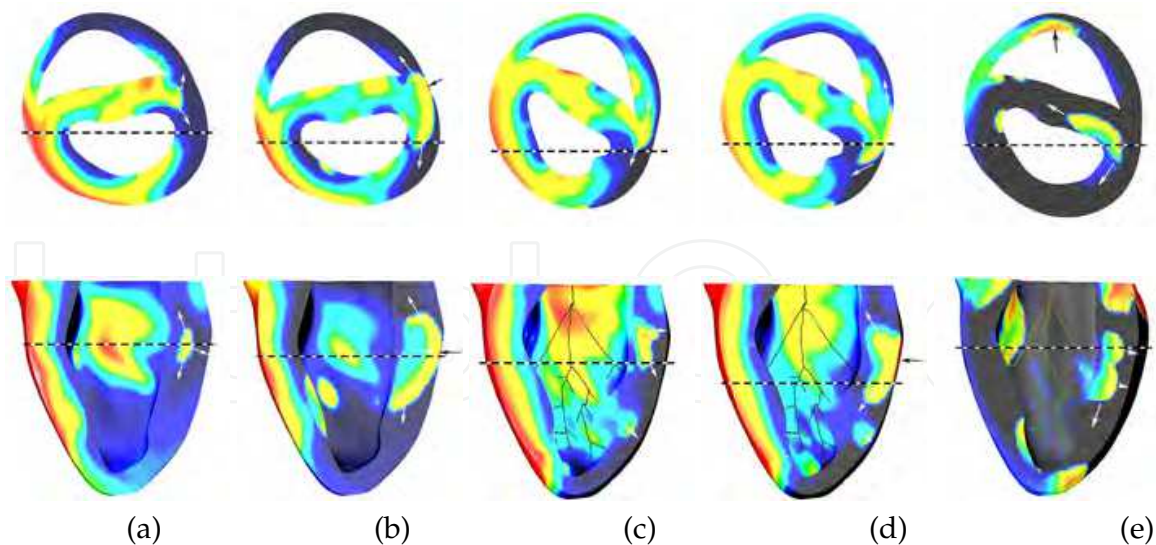
Fig. 7. Transmural postshock activations in the septum (top) and LV free wall (bottom). White arrows indicate the propagation pathways of transmural wavefronts; black arrows indicate epicardial breakthrough sites (a)-(d) or PS-induced propagating activity (e). In (a) and (b), the response to a 10 ms shock is shown in the absence of the PS. Activations originate in the septum and propagate through the free wall. In (c) and (d), similar activations are seen following a 5 ms shock using the AP+PS configuration. Wavefronts originating from PS transmission arrive at the epicardium before shock-induced myocardial wavefronts. (e) shows the response to an even shorter shock (3 ms) for the same configuration. Dashed lines represent cross-section planes relative to the top and bottom views. V_m is shown with the same color scheme used in Fig. 1.

insertion points. While IW abbreviation was indisputable for the fully-penetrating PS, it was less clear for cases where the PS terminated in the midwall. Notably, these cases were subject to a higher degree of variability from sample to sample, which could be the result of surface polarization blocking PS activity.

In our model, rapid conduction through the PS was the source of the epicardial breakthrough terminating the IW. However, there are several limitations and differences with Trayanova's work. We only considered monophasic defibrillation shocks while her group considered biphasic shocks which would lead to different postshock surface states. Our modelling of the PS cell response to large shocks may not be accurate. This is true for all ionic models where behavior outside of the physiological voltage range is not well characterized. If PS conduction became compromised due to a field induced conduction block, or refractory myocardium prevented anterograde transmission across the PMJs, then the tunnel propagation mechanism could account for the IW. In reality, it is likely that both mechanisms play a role, depending on circumstances.

8. Defibrillation

A limited set of computer simulations has been performed with ventricles including a model of the PS(Deo et al., 2009). With an 8 V/cm defibrillation shock, ventricles with a PS were successfully defibrillated while those without a PS were not. The most obvious difference
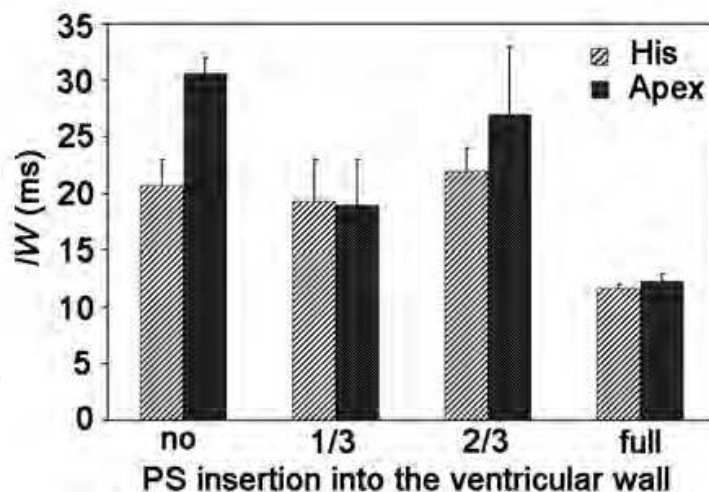
Fig. 8. Effect of PS insertion depth on IW duration. The IW was longest for surface-bound PS and shortest in the case of fibre endpoints that penetrated to the sub-epicardial layer. Error bars correspond to maximum deviation from mean values ($n = 6$).

between the two situations was the more rapid and widespread activation of the epicardium which eliminated excitable gaps. Without the PS, an excitable gap persisted under the anode, allowing reentry to be reinduced. Thus, the PS aided in defibrillation. Experimentally, application of Lugol's solution to the endocardium results in a doubling of DFT(Damiano et al., 1986), suggesting that the PS facilitates defibrillation at lower field strengths.

9. Summary

Based on experimental findings, which are supported by our modelling studies, we conclude that the PS plays a major role in defibrillation. Due to its cable-like nature and complicated geometry, it is excited in many places by an applied electric field, which leads to rapid activation of the entire network. Any excitable gaps are quickly consumed and reentry cannot be reestablishing. This effect is less prominent as shock strength is increased since more myocardium is directly excited by the shock. The complex postshock propagation pattern present with a PS may also play a role in rapid ventricular activation to stop fibrillation.

10. References

Ansari, A., Yen Ho, S. & Anderson, R. H. (1999). Distribution of the Purkinje fibres in the sheep heart, *The Anatomical Record* 254(1): 92–97.

Armiger, L. C. & Knell, C. M. (1988). Fine structural alteration in the atrioventricular junctional conduction tissues of the dog heart during severe ischaemia., *J Submicrosc Cytol Pathol* 20(4): 645–656.

Ashihara, T., Constantino, J. & Trayanova, N. A. (2008). Tunnel propagation of postshock activations as a hypothesis for fibrillation induction and isoelectric window., *Circ Res* 102(6): 737–745.
URL: *http://dx.doi.org/10.1161/CIRCRESAHA.107.168112*

Ashihara, T. & Trayanova, N. A. (2004). Asymmetry in membrane responses to electric shocks: insights from bidomain simulations., *Biophys J* 87(4): 2271–2282.
URL: *http://dx.doi.org/10.1529/biophysj.104.043091*

Canale, E., Campbell, G., Smolich, J. & Campbell, J. (1986). *Cardiac muscle:*, Vol. II, Springer-Verlag, Berlin-Heidelberg-New York-Tokyo, chapter 7, pp. 60–103.

Chattipakorn, N., Fotuhi, P. C., Chattipakorn, S. C. & Ideker, R. E. (2003). Three-dimensional mapping of earliest activation after near-threshold ventricular defibrillation shocks., *J Cardiovasc. Electrophysiol.* 14: 65–69.

Chen, P. S., Shibata, N., Dixon, E. G., Martin, R. O. & Ideker, R. E. (1986). Comparison of the defibrillation threshold and the upper limit of ventricular vulnerability., *Circulation* 73(5): 1022–1028.

Chen, P. S., Shibata, N., Dixon, E. G., Wolf, P. D., Danieley, N. D., Sweeney, M. B., Smith, W. M. & Ideker, R. E. (1986). Activation during ventricular defibrillation in open-chest dogs. evidence of complete cessation and regeneration of ventricular fibrillation after unsuccessful shocks., *J Clin Invest* 77(3): 810–823.
URL: *http://dx.doi.org/10.1172/JCI112378*

Cheng, Y., Mowrey, K. A., Wagoner, D. R. V., Tchou, P. J. & Efimov, I. R. (1999). Virtual electrode-induced reexcitation: A mechanism of defibrillation., *Circ Res* 85(11): 1056–1066.

Constantino, J., Long, Y., Ashihara, T. & Trayanova, N. A. (2010). Tunnel propagation following defibrillation with icd shocks: hidden postshock activations in the left ventricular wall underlie isoelectric window., *Heart Rhythm* 7(7): 953–961.
URL: *http://dx.doi.org/10.1016/j.hrthm.2010.03.026*

Damiano, R. J., Smith, P. K., Tripp, H. F., Asano, T., Small, K. W., Lowe, J. E., Ideker, R. E. & Cox, J. L. (1986). The effect of chemical ablation of the endocardium on ventricular fibrillation threshold., *Circulation* 74(3): 645–652.

Deo, M., Boyle, P., Plank, G. & Vigmond, E. (2009). Arrhythmogenic mechanisms of the purkinje system during electric shocks: a modeling study., *Heart Rhythm* 6(12): 1782–1789.
URL: *http://dx.doi.org/10.1016/j.hrthm.2009.08.023*

Dosdall, D. J., Cheng, K.-A., Huang, J., Allison, J. S., Allred, J. D., Smith, W. M. & Ideker, R. E. (2007). Transmural and endocardial purkinje activation in pigs before local myocardial activation after defibrillation shocks., *Heart Rhythm* 4(6): 758–765.
URL: *http://dx.doi.org/10.1016/j.hrthm.2007.02.017*

Dosdall, D. J., Osorio, J., Robichaux, R. P., Huang, J., Li, L. & Ideker, R. E. (2010). Purkinje activation precedes myocardial activation following defibrillation after long-duration ventricular fibrillation., *Heart Rhythm* 7(3): 405–412.
URL: *http://dx.doi.org/10.1016/j.hrthm.2009.11.025*

Dosdall, D. J., Tabereaux, P. B., Kim, J. J., Walcott, G. P., Rogers, J. M., Killingsworth, C. R., Huang, J., Robertson, P. G., Smith, W. M. & Ideker, R. E. (2008). Chemical ablation of the purkinje system causes early termination and activation rate slowing of long-duration ventricular fibrillation in dogs., *Am J Physiol Heart Circ Physiol* 295(2): H883–H889.
URL: *http://dx.doi.org/10.1152/ajpheart.00466.2008*

Evans, F. G. & Gray, R. (2004). Shock-induced epicardial and endocardial virtual electrodes leading to ventricular fibrillation via reentry, graded responses and transmural activation, *J Cardiovasc. Electrophysiol.* 15: 79–87.

Huelsing, D. J., Spitzer, K. W., Cordeiro, J. M. & Pollard, A. E. (1998). Conduction between isolated rabbit purkinje and ventricular myocytes coupled by a variable resistance., *Am J Physiol* 274(4 Pt 2): H1163–H1173.

Ijiri, T., Ashihara, T., Yamaguchi, T., Takayama, K., Igarashi, T., Shimada, T., Namba, T., Haraguchi, R. & Nakazawa, K. (2008). A procedural method for modeling the purkinje fibers of the heart., *J Physiol Sci* 58(7): 481–486.
URL: *http://dx.doi.org/10.2170/physiolsci.RP003208*

Legrice, I. J., Hunter, P. J. & Smaill, B. H. (1997). Laminar structure of the heart: a mathematical model., *Am J Physiol* 272(5 Pt 2): H2466–H2476.

Li, H. G., Jones, D. L., Yee, R. & Klein, G. J. (1993). Defibrillation shocks produce different effects on purkinje fibers and ventricular muscle: implications for successful defibrillation, refibrillation and postshock arrhythmia., *J Am Coll Cardiol* 22(2): 607–614.

Miquerol, L., Meysen, S., Mangoni, M., Bois, P., van Rijen, H., Abran, P., Jongsma, H., Nargeot, J. & Daniel Gros (2004). Architectural and functional asymmetry of the His-Purkinje system of the murine heart., *Cardiovasc Res* 63: 77-86.

Morley, G. E., Danik, S. B., Bernstein, S., Sun, Y., Rosner, G., Gutstein, D. E. & Fishman, G. I. (2005). Reduced intercellular coupling leads to paradoxical propagation across the purkinje-ventricular junction and aberrant myocardial activation., *Proc Natl Acad Sci U S A* 102(11): 4126–4129.
URL: *http://dx.doi.org/10.1073/pnas.0500881102*

Ono, N., Yamaguchi, T., Ishikawa, H., Arakawa, M., Takahashi, N., Saikawa, T. & Shimada, T. (2009). Morphological varieties of the purkinje fiber network in mammalian hearts, as revealed by light and electron microscopy., *Arch Histol Cytol* 72(3): 139–149.

Sepulveda, N. G., Roth, B. J. & Wikswo, J. P. (1989). Current injection into a two-dimensional anisotropic bidomain., *Biophys J* 55(5): 987–999.
URL: *http://dx.doi.org/10.1016/S0006-3495(89)82897-8*

Sobie, E. A., Susil, R. C. & Tung, L. (1997). A generalized activating function for predicting virtual electrodes in cardiac tissue., *Biophys J* 73(3): 1410–1423.
URL: *http://dx.doi.org/10.1016/S0006-3495(97)78173-6*

Streit, J. (1987). Effects of hypoxia and glycolytic inhibition on electrical properties of sheep cardiac purkinje fibres., *J Mol Cell Cardiol* 19(9): 875–885.

Trayanova, N. & Skouibine, K. (1998). Modeling defibrillation: effects of fiber curvature., *J Electrocardiol* 31 Suppl: 23–29.

Vetter, F. & McCulloch, A. (1998). Three-dimensional analysis of regional cardiac function: a model of rabbit ventricular anatomy., *Prog Biophys Mol Biol* 69(2-3):157–183.

Vigmond, E. J. & Clements, C. (2007). Construction of a computer model to investigate sawtooth effects in the purkinje system., *IEEE Trans Biomed Eng* 54(3): 389–399.
URL: *http://dx.doi.org/10.1109/TBME.2006.888817*

Vigmond, E. J., dos Santos, R. W., Prassl, A. J., Deo, M. & Plank, G. (2008). Solvers for the cardiac bidomain equations., *Prog Biophys Mol Biol* 96(1-3): 3–18.
URL: *http://dx.doi.org/10.1016/j.pbiomolbio.2007.07.012*

Wiedmann, R. T., Tan, R. C. & Joyner, R. W. (1996). Discontinuous conduction at purkinje-ventricular muscle junction., *Am J Physiol* 271(4 Pt 2): H1507–H1516.

Wu, T.-J., Lin, S.-F., Hsieh, Y.-C., Chiu, Y.-T. & Ting, C.-T. (2009). Repetitive endocardial focal discharges during ventricular fibrillation with prolonged global ischemia in isolated rabbit hearts., *Circ J* 73(10): 1803–1811.
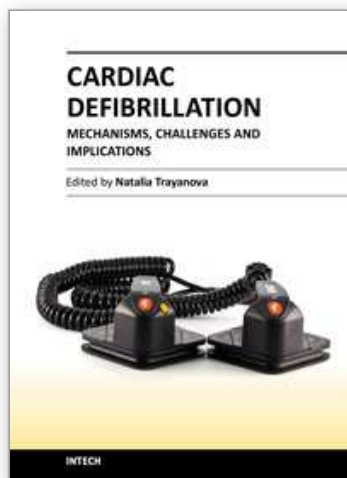
Cardiac Defibrillation - Mechanisms, Challenges and Implications

Edited by Prof. Natalia Trayanova

The only known effective therapy for lethal disturbances in cardiac rhythm is deï¬brillation, the delivery of a strong electric shock to the heart. This technique constitutes the most important means for prevention of sudden cardiac death. The efficacy of defibrillation has led to an exponential growth in the number of patients receiving implantable devices. The objective of this book is to present contemporary views on the basic mechanisms by which the heart responds to an electric shock, as well as on the challenges and implications of clinical defibrillation. Basic science chapters elucidate questions such as lead configurations and the reasons by which a defibrillation shock fails. Chapters devoted to the challenges in the clinical procedure of defibrillation address issues related to inappropriate and unnecessary shocks, complications associated with the implantation of cardioverter/defibrillator devices, and the application of the therapy in pediatric patients and young adults. The book also examines the implications of defibrillation therapy, such as patient risk stratification, cardiac rehabilitation, and remote monitoring of patient with implantable devices.

How to reference

In order to correctly reference this scholarly work, feel free to copy and paste the following:

Edward J Vigmond, Patrick M. Boyle and Makarand Deo (2011). The Role of the Purkinje System in Defibrillation, Cardiac Defibrillation - Mechanisms, Challenges and Implications, Prof. Natalia Trayanova (Ed.), ISBN: 978-953-307-666-9, InTech, Available from: http://www.intechopen.com/books/cardiac-defibrillation-mechanisms-challenges-and-implications/the-role-of-the-purkinje-system-in-defibrillation

INTECH
open science | open minds